# Technical Note

# Real time forecast service for geomagnetically induced currents

# WP300: Computation of GIC from the geomagnetic field

Ari Viljanen [1], Magnus Wik [2], Risto Pirjola [1,3] and Antti Pulkkinen [1,4]

[1] Finnish Meteorological Institute, Helsinki, Finland
[2] Swedish Institute of Space Physics, Lund, Sweden
[3] Now at Natural Resources Canada
[4] Now at NASA Goddard Space Flight Center, United States

January 10, 2006

# Abstract

The purpose of this study is to provide a routine tool for calculating geomagnetically induced currents (GIC) in the southern part of the Swedish 400 kV power grid. As input we assume that geomagnetic recordings are available at the nearby region for calculating the geoelectric field. The necessary power grid information consists of the topology of the system and of the resistance values of the transformers and transmission lines as well as the locations of the earthing points.

The initial geoelectric field was calculated assuming a 2-layer conductivity model of the earth: thickness of the upper layer 150 km and its resistivity 40 Ωm; the resistivity of the lower layer 0.4 Ωm. The geomagnetic field interpolated at a regular grid covering the power system was then multiplied by the surface impedance to get the geoelectric field. Since there are presently no magnetic observatories in the region, we also investigated the spatial variability of the magnetic and electric fields there.

GIC recordings were available at one site. Assuming a uniform electric field, the modelled GIC at this site is $GIC = (-53.3E_x + 150.9E_y)$ Akm/V. Using four disturbed events, we found that multiplying the initial electric field by 3.89 gives the best fit of the model in the least-square sense. This yielded the median relative error of 58% when timesteps with the measured GIC exceeding 5 A were considered.

# Contents

# 1 Introduction

The Space Research Unit of the Finnish Meteorological Institute is involved in three service development activities (SDA) within the ESA Space Weather Pilot Programme:

- Auroras Now! and GIC Now! (PI: FMI)
- Real Time Forecast Service for Geomagnetically Induced Currents (PI: IRF-Lund, Sweden)
- Real-Time GIC Simulator (PI: Natural Resources Canada)

WP300 of "Real Time Forecast Service for Geomagnetically Induced Currents" deals with the calculation of GIC in a power system. This technical note describes the methods and software used for that purpose. The map of the whole power system in northern Europe is shown in Fig. 1. This WP deals with a small part of it in southern Sweden.

## 1.1 Definitions, acronyms and abbreviations

FFT = Fast Fourier Transform
FMI = Finnish Meteorological Institute
GIC = geomagnetically induced current
IRF = Swedish Institute of Space Physics
SDA = service development activity
WP = work package

$\mathbf{E} = E_x\mathbf{e}_x + E_y\mathbf{e}_y$ = horizontal electric field vector ($x$ to the geographic north, $y$ to the east)
$\mathbf{H} = B_x\mathbf{e}_x + B_y\mathbf{e}_y$ = horizontal magnetic field vector
$d\mathbf{H}/dt$ = time derivative of $\mathbf{H}$

## 1.2 Structure of this document

We first present briefly the method of calculating the geoelectric field (Sect. 2.1). The basic input is the interpolated magnetic field in the region under study obtained from WP200. Since there are no observatories in southern Sweden,

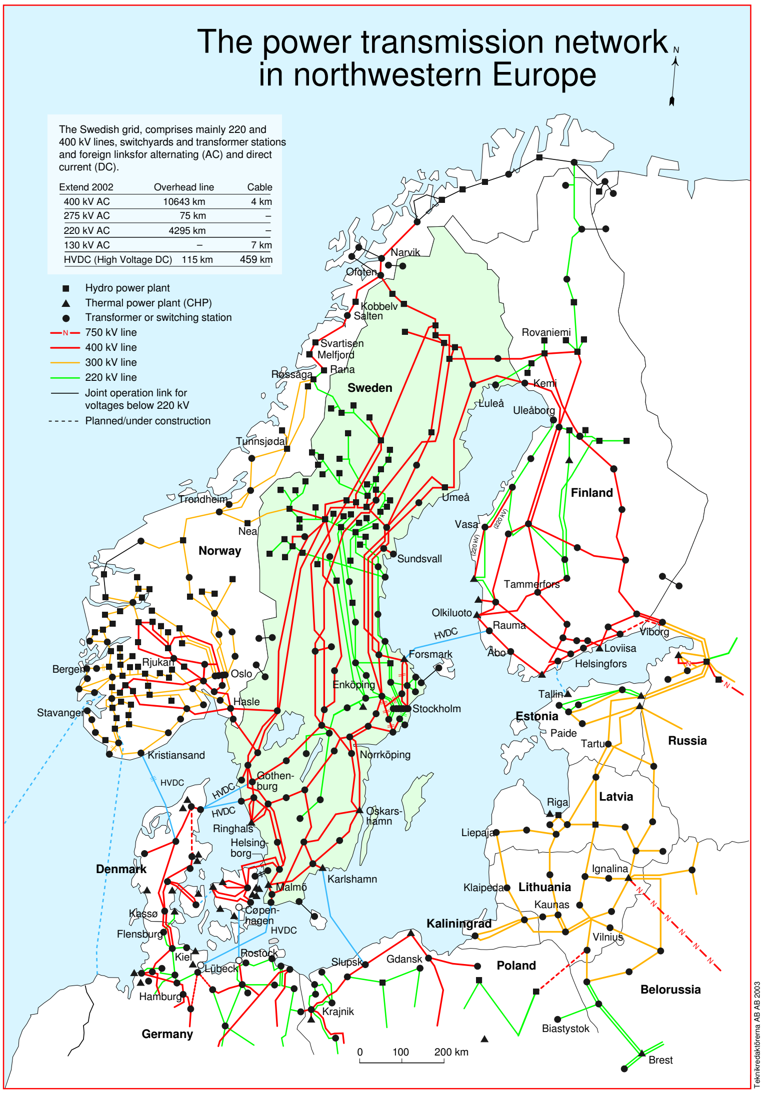


Figure 1: The high-voltage power transmission system in Nordic countries.

we study the spatial variability of the magnetic and electric fields (Sect. 2.2). Modelling of GIC is described in Sect. 3. We first derive an empirical relationship between the modelled electric field and the measured GIC (Sect. 3.1). This serves as one way to verify the results of the direct network modelling in Sect. 3.2.

# 2 Calculation of the geoelectric field

It is conventional to divide GIC modelling into two independent parts:
1. Determination of the geoelectric field.
2. Calculation of GIC using the given geoelectric field.
This section deals with the first step.

## 2.1 Local plane wave method

The simplest way to determine the geoelectric field from geomagnetic recordings is to apply the local plane wave model (Viljanen et al., 2004). This means that the surface electric field is related to the local geomagnetic field by the surface impedance $Z(\omega)$:

$$E_x(\omega) = Z(\omega)B_y(\omega)/\mu_0,\ E_y(\omega) = -Z(\omega)B_x(\omega)/\mu_0 \tag{1}$$

where $\omega$ is the angular frequency and $\mu_0$ is the vacuum permeability. The time-domain values are obtained by the Fourier transform (FFT in computer executions). With a special case of a uniform earth with conductivity $\sigma$, the time-domain formula is

$$E_x(t) = \frac{1}{\sqrt{\pi\mu_0\sigma}} \int_{-\infty}^{t} \frac{g_y(u)}{\sqrt{t-u}},\ E_y(t) = -\frac{1}{\sqrt{\pi\mu_0\sigma}} \int_{-\infty}^{t} \frac{g_x(u)}{\sqrt{t-u}} \tag{2}$$

where $g(t) = dB(t)/dt$ is the time derivative of the magnetic field. These expressions show explicitly that the electric field depends on all previous values of the magnetic field, although the most recent ones have the largest effect. It is also obvious that $dB/dt$ is a reasonable indicator of GIC activity (Viljanen et al., 2001).

The surface impedance depends on the local 1-D conductivity structure of the earth. We assume here that the same model can be used in whole study region. However, it is also possible to refine the method by selecting

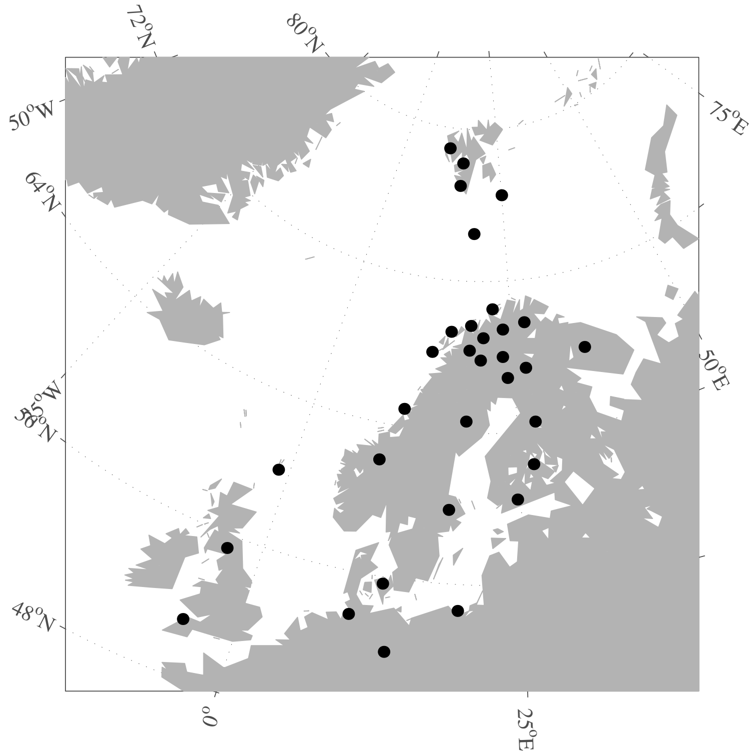


Figure 2: Magnetometer stations used for the magnetic field interpolation in southern Sweden.

different 1-D models for different sites. As a starting point of earth models, we can use the results by Korja et al. (2002) which indicate typical values in the Fennoscandian Shield. A quantitative fitting of the local conductivity model requires measured GIC values.

The magnetic field is recorded continuously at several sites in northern Europe (Fig. 2). The most convenient way to provide the electric field input to GIC programs is to use a regular grid covering the power system studied. So the first step is to interpolate the magnetic field on the same grid (Fig. 3). This is described in the technical note of WP 200, and the interpolation method is documented in Pulkkinen (2003) and Pulkkinen et al. (2003a).

We have used here a much wider magnetometer network than would be necessary for studies in southern Sweden. However, the database is now readily available for possible later extensions to other parts of Sweden or

Table 1: Days used in this study.

| no. | UT day | no. | UT day | no. | UT day |
|---|---|---|---|---|---|
| 01 | 19980924 | 11 | 19991012 | 21 | 20000710 |
| 02 | 19980925 | 12 | 19991022 | 22 | 20000711 |
| 03 | 19981002 | 13 | 19991028 | 23 | 20000713 |
| 04 | 19981020 | 14 | 19991112 | 24 | 20000714 |
| 05 | 19990815 | 15 | 20000122 | 25 | 20000715 |
| 06 | 19990820 | 16 | 20000211 | 26 | 20000719 |
| 07 | 19990830 | 17 | 20000224 | 27 | 20000812 |
| 08 | 19990922 | 18 | 20000406 | | |
| 09 | 19990926 | 19 | 20000523 | | |
| 10 | 19991010 | 20 | 20000608 | | |

neighbouring countries. Furthermore, the same data are useful for scientific investigations too. The 27 days used here for statistical studies are listed in Table 1.

In the practical computation, we take a finite sample of the magnetic field time series. We apply a window function to the data to force the first and last values of the sample to be equal to reduce the Gibbs phenomenon always related to Fourier series. We have used the Parzen window:

$$W = 1 - [\frac{2(n - N/2)}{N}]^8 \tag{3}$$

for $n = 1, ..., N$ and $W = 0$ otherwise.

## 2.2 Spatial uniformity of the geoelectromagnetic field

As desribed in the previous section, the geoelectric field is obtained conveniently as follows (Viljanen et al., 2004):
1. Interpolate the magnetic field on a grid covering the area of interest.
2. Select a 1-D conductivity model for each grid point. (In this work, we have assumed the same model for the whole area.)
3. Calculate the electric field by Eq. 1.

The purpose of this section is to demonstrate that the electric field is spatially rather uniform in southern Sweden when considering length scales

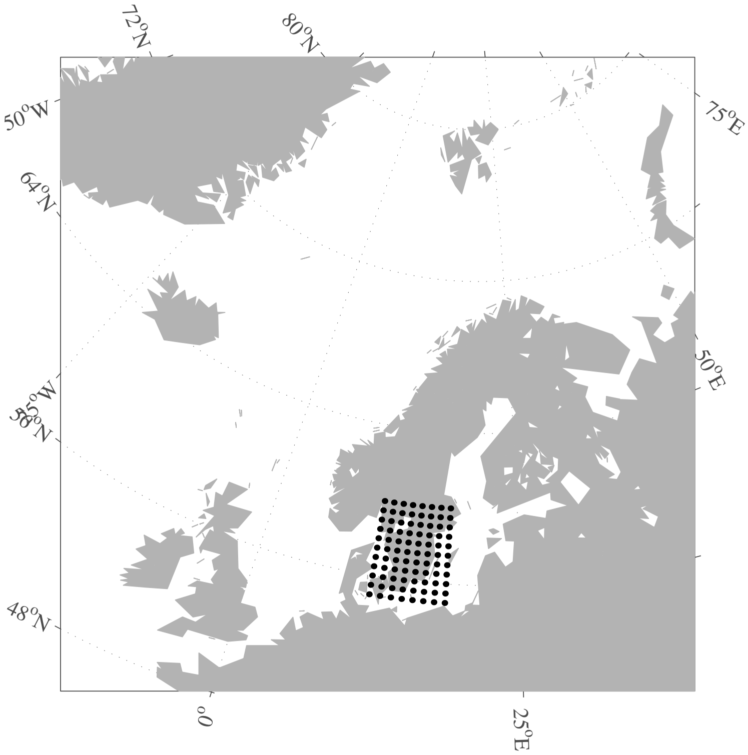


Figure 3: The dense grid covering southern Sweden. There are 88 grid points.

of the order of 100 km. This is expected, since Viljanen et al. (2004) showed that in southern Finland the geoelectric field is spatially quite uniform in the east-west direction in an area of a 100-200 km length scale. Southern Sweden is located farther from the auroral region, so a similar result is evident. A practical consequence is that even a single magnetometer suitably located in the centre of the region of interest provides good estimates of GIC. This is utilized in GIC Now! which produces nowcasted GIC in the Finnish natural gas pipeline system from the data of the Nurmijärvi Geophysical Observatory.

Concerning southern Sweden, we show here that a reasonable modelling of GIC is possible even though the closest magnetometers are presently located in Brorfelde (Denmark) and Uppsala. The new instrument being installed in Växjö would still improve the interpolation of the field. It would also be possible to use only data from this new site to provide nowcasts for the whole

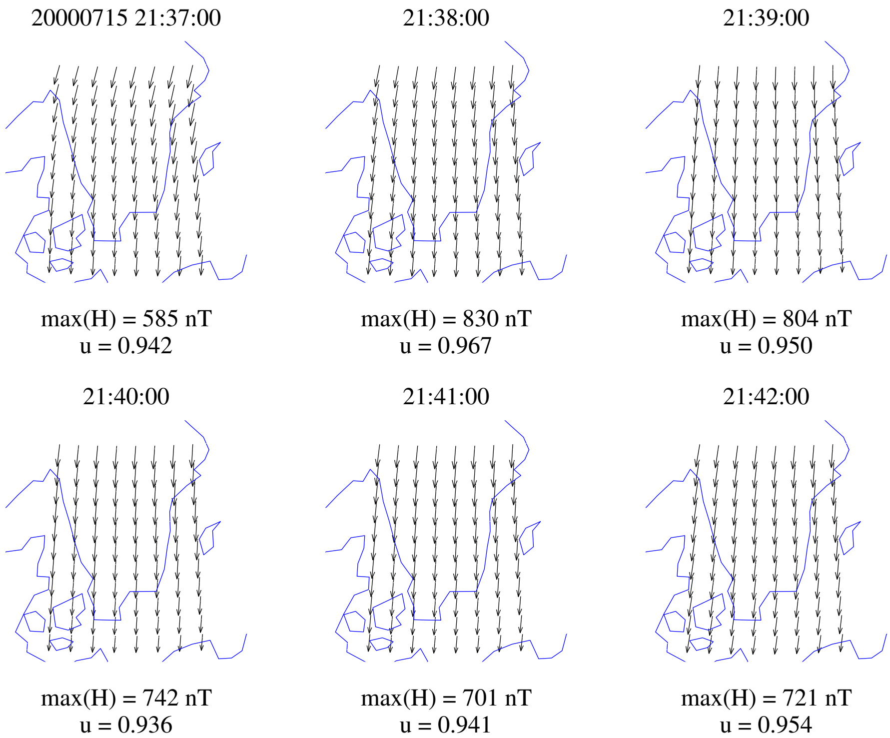


Figure 4: Snapshots of interpolated horizontal magnetic field vectors. The uniformity of the field is given by the quantity $u$ (Eq. 4).

southern Sweden.

Examples of the input magnetic field (horizontal component $\mathbf{H}$), its time derivative and the calculated electric field are shown in Figs. 4-6. The event is selected during a period with large $d\mathbf{H}/dt$ values in the region. A typical feature is that the magnetic field is spatially very uniform, whereas $d\mathbf{H}/dt$ is more structured. This is related to small-scale ionospheric currents with a relatively uniform main flow in background (Pulkkinen et al., 2003b). The pattern of the horizontal electric field is roughly obtained from $d\mathbf{H}/dt$ by a 90 degrees counterclockwise rotation. However, this is not a one-to-one relationship, but the history of $d\mathbf{H}/dt$ affects the detailed structure (Eq. 2). In other words, the earth affects as a filter smoothing the most rapid temporal variations of $d\mathbf{H}/dt$.

To measure the spatial uniformity of the field, we calculate the difference

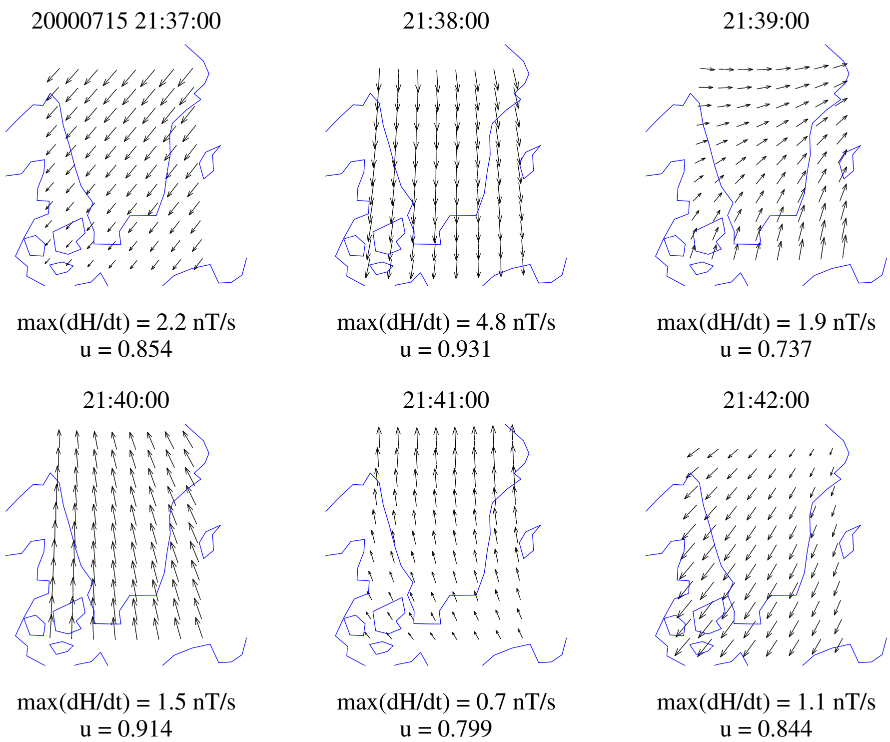


Figure 5: As Fig. 4, but for the interpolated time derivative of horizontal magnetic field vectors.

of $\mathbf{H}$ between each pair of sites and compare it to the sum of magnitudes of $\mathbf{H}$:

$$u(t) = 1 - \frac{2}{N(N-1)} \sum_{m=1}^{N} \sum_{n=m+1}^{N} \frac{|\mathbf{H}_m(t) - \mathbf{H}_n(t)|}{|\mathbf{H}_m(t)| + |\mathbf{H}_n(t)|} \qquad (4)$$

where $\mathbf{H}_m(t)$ is given at site $m$ at time $t$ and $N$ is the total number of sites. If the field is completely uniform then $u = 1$. Note that with the normalization used in Eq. 4, $u$ can vary only between 0 and 1, because $0 \leq |\mathbf{a}-\mathbf{b}| \leq |\mathbf{a}|+|\mathbf{b}|$, when the double sum is at most $N(N-1)/2$.

Uniformity indicators during one day are shown in Figs. 7-9 using the same definition for $\mathbf{H}$, $d\mathbf{H}/dt$ and $\mathbf{E}$. Visual inspection shows that, despite its simplicity, $u$ is a reasonable indicator. Statistical results are presented in Fig. 10. Both single day results and statistical results show that $\mathbf{H}$ is quite smooth whereas $d\mathbf{H}/dt$ and $\mathbf{E}$ are more variable. Statistical results

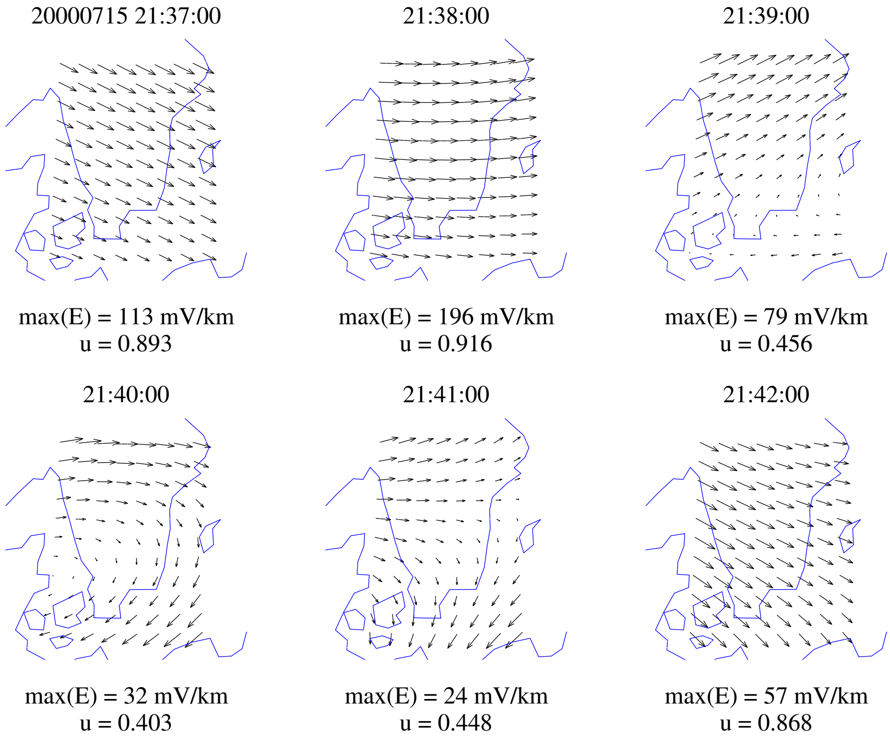


Figure 6: As Fig. 4, but for the calculated geoeletric field.

show that **E** is also spatially slightly more uniform than $d\mathbf{H}/dt$. There is no obvious correlation between the amplitude of the field and the spatial uniformity (Figs. 7-9).

Although these results indicate that the electric field is spatially a little smoother than the time derivative of the magnetic field, a careful interpretation is necessary. First of all, we have assumed the same conductivity model throughout the region. Although in a large scale this seems to be a good assumption in southern Sweden (Korja et al., 2002, Fig. 9), there are always very small-scale anomalies. It follows that a pointwise measured electric field has a rapid spatial variation (even in the scale of one km), whereas the magnetic field is less affected. The physical reason is that lateral conductivity anomalies cause charge accumulation, so the electric field is affected both by charges and currents; the magnetic field is only caused by currents. The model calculations above assume a layered earth, when there is no charge

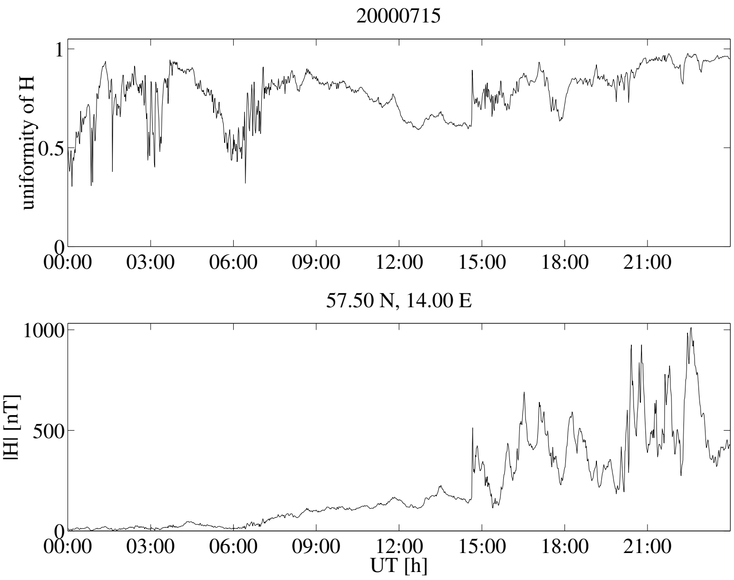


Figure 7: Upper panel: Uniformity of the interpolated horizontal magnetic field on July 15, 2000, in the dense grid of Fig. 3. Lower panel: Magnitude of the horizontal field in the centre of the grid.

accumulation at all. In other words, these calculations show that the nonuniformity of the electric field due to spatially varying ionospheric currents is not very large in this region.

A natural question is whether simple layered earth models are adequate. This seems to be the case, because GIC at a given site is not related to the local electric field at the same site, but to the regional average. GIC is driven by voltages obtained by integrating the electric field along power lines. Integration is a spatially smoothing operation, so small-scale anomalies are not significant. Furthermore, when a given site is considered then it is not necessary to know the electric field at distant regions, but the area defined by the nearest earthing points is dominating. Experiences in modelling GIC in the Finnish power system and natural gas pipeline support these conclusions (Viljanen et al., 2004).

Finally, we should note that the conclusions for southern Sweden are not necessarily valid for higher latitudes close to the auroral region. We expect a stronger inhomogeneity of all fields there due to the vicinity of

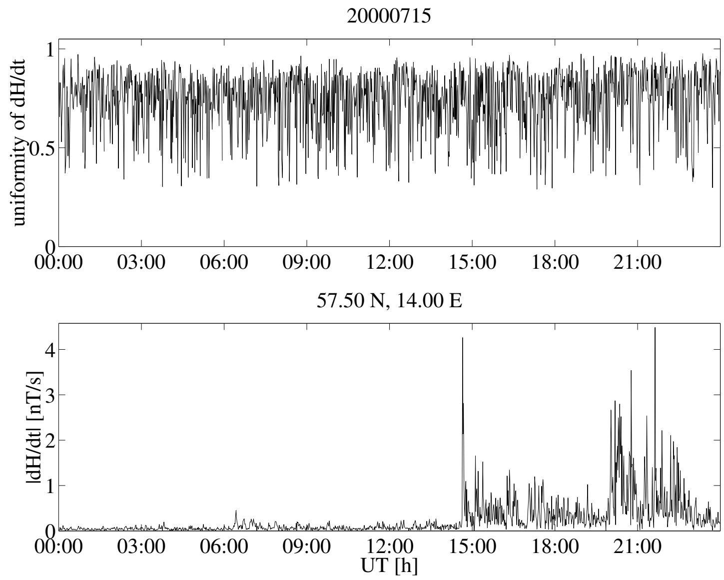


Figure 8: Upper panel: Uniformity of the interpolated time derivative of the horizontal magnetic field on July 15, 2000, in the dense grid of Fig. 3. Lower panel: Magnitude of the time derivative of the horizontal field in the centre of the grid.

more complicated ionospheric currents (Viljanen et al., 2001).

# 3 Calculation of GIC from the electric field

As already mentioned, GIC modelling consists of two independent parts:
1. Determination of the geoelectric field.
2. Calculation of GIC using the given geoelectric field.

The second step requires that the electromagnetic parameters and the topology of the power system are known. Because GIC is a low-frequency phenomenon (compared to the 50 Hz AC frequency), a DC model is sufficient (Pulkkinen, 2003). The basic modelling technique applied here is presented by Lehtinen and Pirjola (1985).

GIC at a given site produced by a spatially uniform electric field is

$$GIC(t) = aE_x(t) + bE_y(t) \tag{5}$$

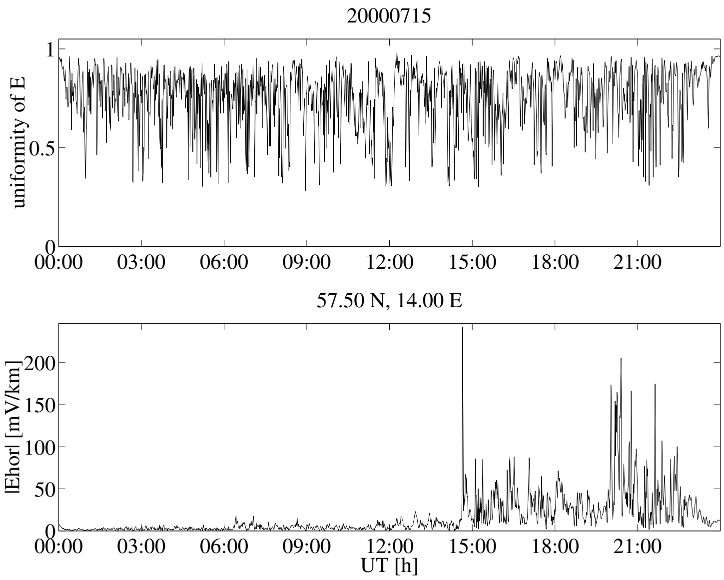


Figure 9: Upper panel: Uniformity of the calculated geoeletric field on July 15, 2000, in the dense grid of Fig. 3. Lower panel: Magnitude of the horizontal electric field in the centre of the grid.

where $E_x, E_y$ are the north and east components of the electric field. The coefficients $a$ and $b$ depend only on the geometry and resistances of the power system. So for a fixed network, they must be determined only once, which makes computations very fast. If the electric field varies spatially then it must be integrated along power lines separately for each timestep, and no simple relationship like Eq. 5 exists.

## 3.1 Empirical modelling based only on measured data

Equation 5 also allows for a straighforward determination of GIC without an explicit power system model. Then we need the electric field at a nearby location to the GIC site, and measured GIC values. Assumption of a spatially uniform electric field is used too, which is reasonable based on the results of Sect. 2.2. It is also necessary that the configuration of the power grid does not change during the period studied, because that would affect $a$ and $b$. We applied this approach to the GIC data at a Swedish transformer in

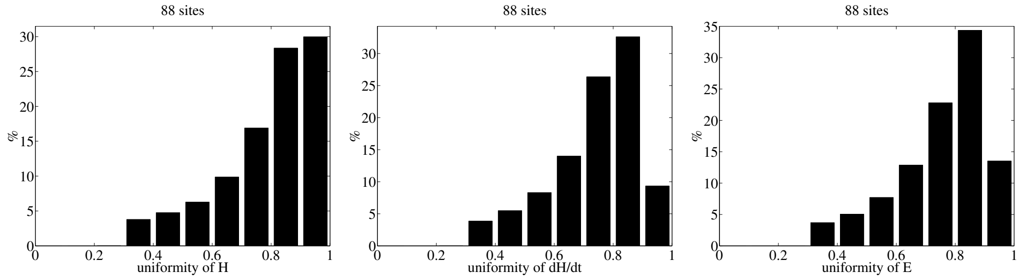


Figure 10: Distribution of the uniformity parameter $u$ in Eq. 4 for the days in Table 1. Plots from left to right: the interpolated horizontal magnetic field, its time derivative, and the calculated geoelectric field.

1998-2000 (Table 1), and fitted the coeffiecients $a$ and $b$ in Eq. 5 minimising the difference between modelled and measured GIC. We used the modelled geoelectric field at the point 57 N, 16 E. We assumed the following two-layer earth model: thickness of the upper layer 150 km and its resistivity 40 $\Omega$m; the resistivity of the lower layer 0.4 $\Omega$m. Using another model would affect the coefficients $a$ and $b$ too.

Because large GIC values are most important, we considered only time-steps with the measured $|GIC| > 10$ A in the fitting. Furthermore, the accuracy of GIC data is only 1 A, so it is not meaningful to use GIC values of only a few amperes. The empirical relation between GIC and the electric field is

$$GIC(t) = -160E_x(t) + 687E_y(t) \tag{6}$$

The electric field is given in V/km and GIC is obtained in amperes. We use the convention that GIC is positive when it flows into the ground. This formula is approximately valid in the period Sep 1998 - Oct 2000. The result shows that GIC at this site was mainly determined by the eastward component of the electric field, which in turn is closely related to the time derivative of the northward magnetic field ($dX/dt$).

The measured GIC time series was shifted two minutes backwards due to an obvious timing error. This shift provided the smallest fitting error and also yielded the best visual correspondence of modelled and measured GIC curves.

The median model error for $|GIC| > 10$ A was 10.3 A, which is quite large. This may be due to occasional changes in the power grid near the

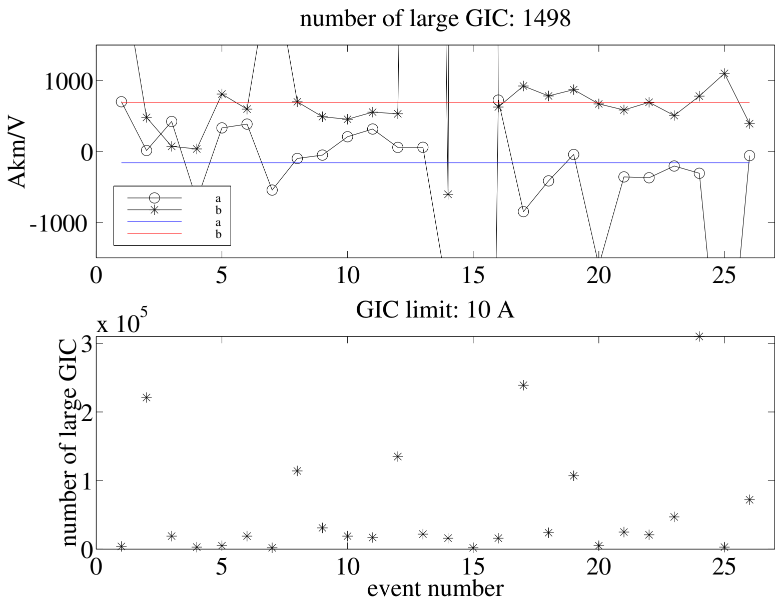


Figure 11: The upper panel shows the event-to-event variability of the multipliers $a$ (circle) and $b$ (asterisk) in Eq. 5. The "global" values in Eq. 6 are shown as blue ($a$) and red ($b$) lines. The number of large GIC values used in each event is shown in the lower panel.

GIC site, or due to measurement problems. The event-to-event variability is quite large as shown in Fig. 11. However, when a large number of GIC values were available, the single event multipliers $a$ and $b$ are close to the "global" values. A clear exception is the big storm of April 6, 2000, when the modelled values are much smaller than the measured ones. We also studied the effect of different GIC thresholds on the coefficients $a$ and $b$ and on the fitting error. The results are shown in Table 2. It is clear that the empirical fitting is not an optimal solution in this case.

## 3.2 Full network modelling

The power grid data obtained from the Swedish power company included station coordinates (in a special Swedish $xyz$ coordinate system), resistances of each parallel transformer at the stations considered, transmission line resistances and station earthing resistances. Information about autotransformers

Table 2: Empirical coefficients $a$ and $b$ (Eq. 5, unit A·km/V) with different limits of large GIC values used in the fit. The second column gives the number of usable timesteps.

| limit [A] | # | $a$ | $b$ | median error [A] | rel. error [%] |
|---|---|---|---|---|---|
| 5 | 3387 | -64 | 612 | 5.7 | 69 |
| 10 | 1498 | -160 | 687 | 10.3 | 67 |
| 15 | 845 | -286 | 761 | 13.7 | 63 |
| 20 | 556 | -336 | 821 | 17.9 | 62 |
| 30 | 271 | -574 | 933 | 23.4 | 58 |

between the 400 kV and 130 kV grids was also given.

GIC calculations were limited to the 400 kV system at the first stage and special attention was paid to a station in southern Sweden, at which GIC is continuously recorded. The data provided by the power company were limited to the part of the entire grid that is necessary for calculating GIC at the particular station. All stations directly connected to the specific site (nearest neighbours) by a transmission line and their nearest neighbours were taken into account (cf. Pirjola, 2005). The size of the grid modelled at this stage contains 14 stations and 17 lines (Fig. 12). We assume the lines to be straight between the stations. Specifically, if a spatially uniform electric field is used then the shapes of the lines do not matter at all.

To ensure that there were no evident errors in power system input data, two different and independent GIC computation codes with a uniform electric field assumption were used, and both of them gave the same results. Other test calculations concerned the rotation of a uniform field to identify at each station the field direction that gives the largest GIC there, and the relative magnitudes of these largest GIC values were also obtained. As expected, the tests showed that the largest GIC were observed at corners and ends of the system, which is illustrated in Fig. 13.

The uniform field coefficients in Eq. 5 calculated from the network model for the specific station are $a = -53.3$ Akm/V and $b = 150.9$ Akm/V, i.e.

$$GIC = -53.3E_x + 150.9E_y \tag{7}$$

Comparison to the empirical values (Eq. 6) confirms the dominance of the eastward electric field.

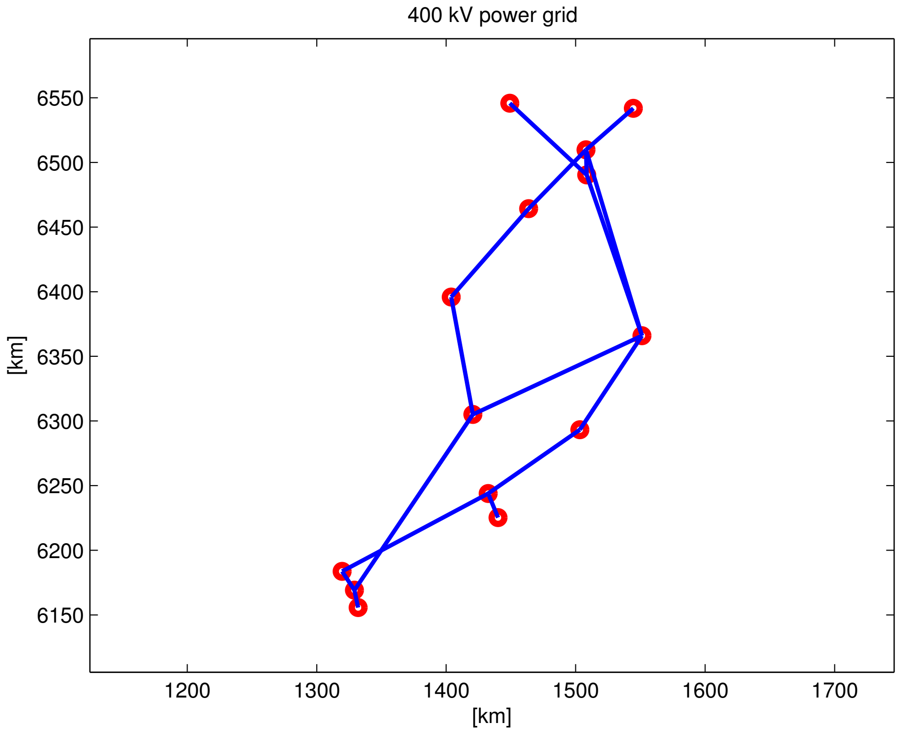


Figure 12: Simplified model of the 400 kV power system in southern Sweden.

The events given in Table 1 were also considered by first calculating the geoelectric field from spatially interpolated geomagnetic data by using the two-layer earth conductivity model mentioned in Sect. 3.1. The electric field was calculated on a grid with each cell of size 30 km x 30 km. The agreement with GIC measurements was satisfactory in the least-square difference sense after the computed GIC values were multiplied by 3.89 to compensate shortcomings of the initial conductivity model.

An example of modelling of a single event are shown in Fig. 14. The modelled GIC generally follows well the measured one, but there are at times quite large deviations in magnitudes. This is also reflected into the distribution of the modelling error shown in Fig. 15. The most obvious reason for these differences is quite a large distance to the nearest magnetic observatory. The transformer station considered is located approximately in the midpoint

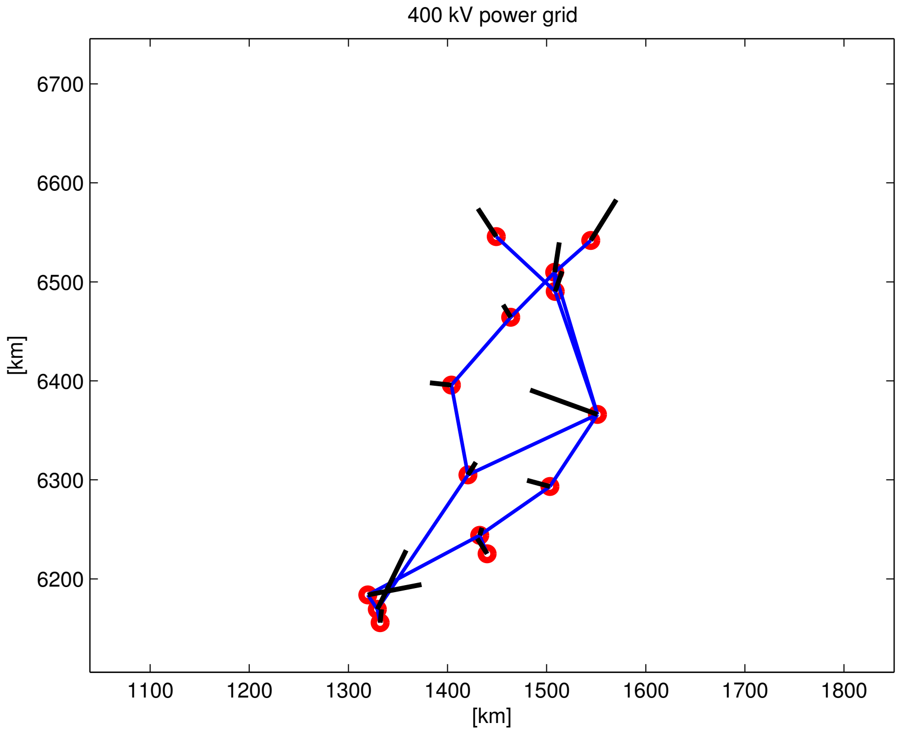


Figure 13: The direction of the uniform electric field which creates the largest GIC at each 400 kV station. The amplitude of GIC is proportional to the length of the arrow.

between Brorfelde and Uppsala, so the latitudinal variation of the magnetic field cannot be exactly captured. Another error source is the possibility of a temporary change in the power system close to the station like a short-time disconnection of a transmission line. That would affect the coefficients in Eq. 7.

As a comparison to a similar system, we refer to GIC Now! SDA for the Finnish natural gas pipeline network, where the median relative nowcasting error is only 30%. That success is evidently due to the favourable near location of the magnetic observatory to the pipeline and the GIC recording site.

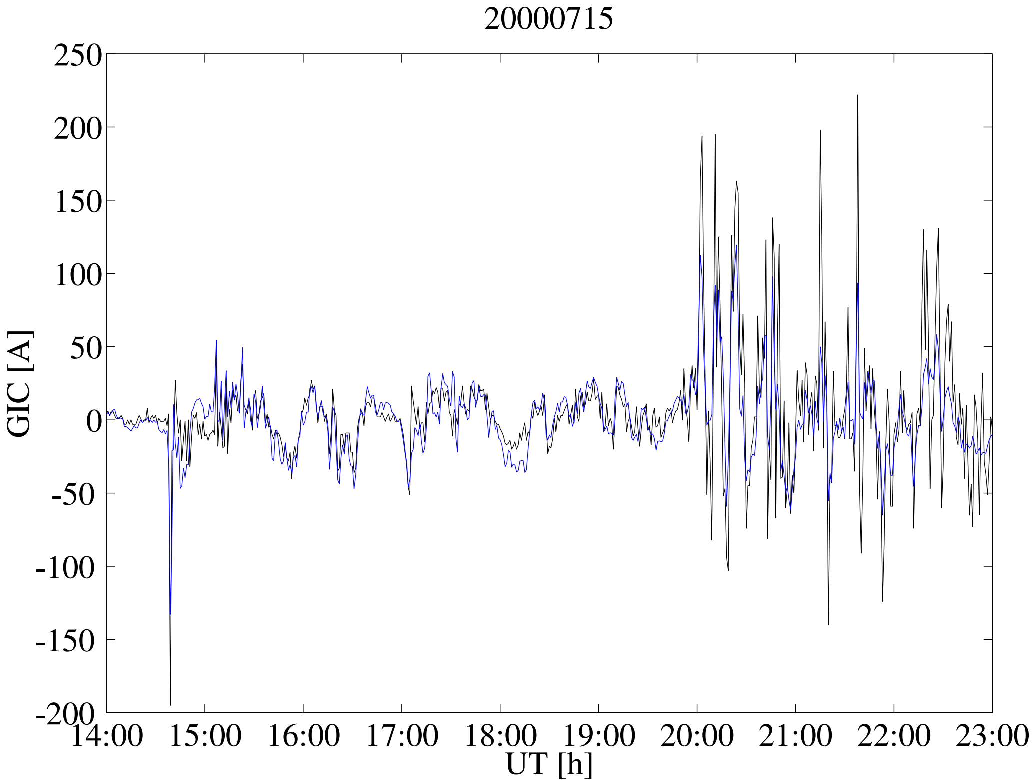


Figure 14: Measured (black) and modelled (blue) GIC on July 15, 2000, at a 400 kV transformer station in southern Sweden.

# 4 GIC software

## 4.1 General

We have used previuously developed software for the calculation of GIC in the Swedish power system. Only some minor fine-tuning has been necessary. Another set of programs was written during the SDA to perform statistical analysis of the measured GIC data in the specific case of Sweden. The latter programs are also extensively based on older routines developed at FMI.

MatLab is an optimal software environment, since the GIC calculation from a given geoelectric field in a known power grid is convenient to write in a matrix form (Lehtinen and Pirjola, 1985).

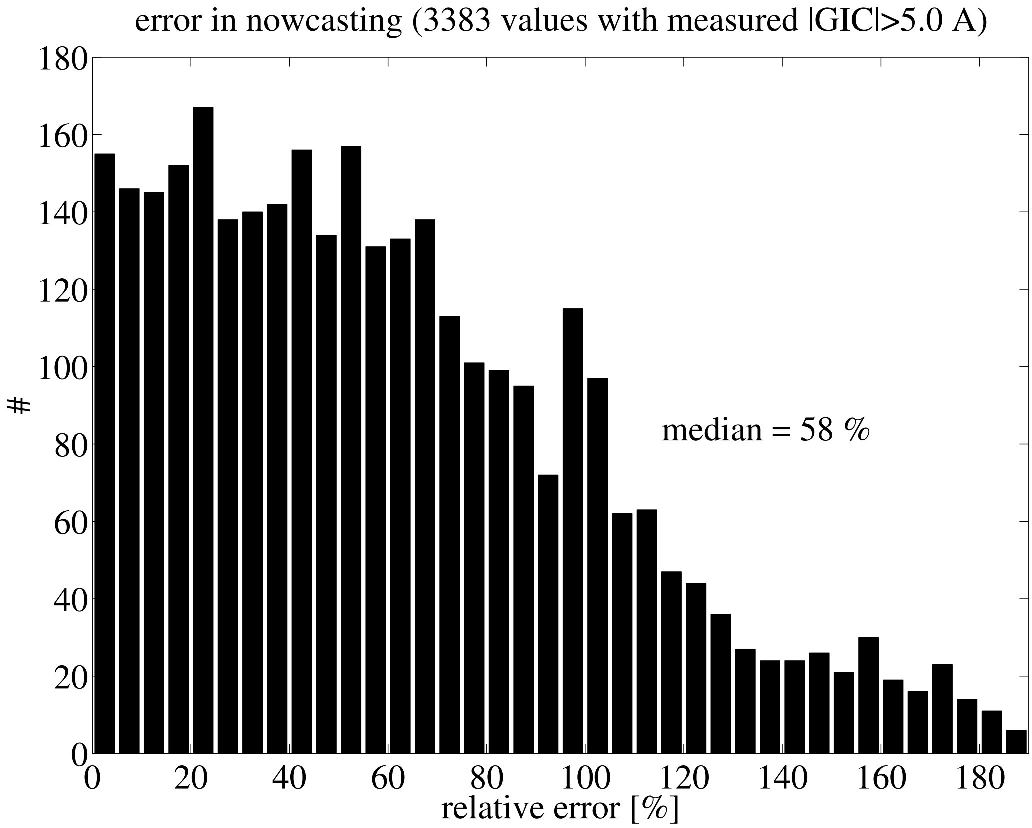


Figure 15: The distribution of the relative error between the modelled and measured GIC. Timesteps with the measured GIC exceeding 5 A have been included. The horizontal axis is cut at 190 %, but there are some larger relative errors too.

## 4.2 List of MatLab files

- exey_irf.m
  The main routine to calculate the electric field from the interpolated magnetic field of the selected set of events.

- exey_calc_irf.m
  Subroutine for exey_irf.m to calculate the surface impedance and the electric field.

- plot_irf.m
  Plotting routine for the magnetic and electric fields of a single day.

- bxby_stat_irf.m
  Routine for a statistical analysis of the interpolated magnetic field of the selected set of events.

- exey_stat_irf.m
  Routine for a statistical analysis of the calculated magnetic field of the selected set of events.

- Network_Map.m
  Routine for a schematic plotting of the Swedish power network.

- plot_gicdata_irf.m
  Simple plotting routine for the measured GIC. The program has also an option to save plots as eps files and to write automatically a LaTeX file containing these figures.

- power_GIC.m
  Routine for calculating earthing and line GIC in the Swedish system produced by a uniform eastward/northward geoelectric field of 1 V/km.

- GIC_rotation.m
  Routine for calculating GIC in the Swedish system due to an electric field of 1 V/km having any direction. Uses the results of power_GIC.m.

- Largest_GIC_arrows.m
  Routine for finding for each station the geoelectric field direction that gives the largest GIC at this station and makes a plot showing these directions. Uses the result of GIC_rotation.m.

- fit_gicexey_irf.m
  Routine for fitting coefficients $a$ and $b$ in Eq. 5. The electric field calculated by exey_irf.m and the measured GIC data are needed as input. The program has also an option to save plots of measured and modelled GIC as eps files and to write automatically a LaTeX file containing these figures.

Calculation of the electric field for one day (1440 one-minute values) at 88 sites takes a few seconds on a Macintosh PowerBook G4 with a 867 MHz processor. Statistical analysis of the fields (of 27 days) takes a few minutes.

## 4.3 Data formats

The interpolated magnetic field is stored in MatLab binary files named as interpBYYYYMMDD.mat (YYYYMMDD = year, month, day). It contains the following variables:

$BX, BY, BZ$: geographic north, east and downwards components of the magnetic field ($NxM$ matrices, each row corresponding to one timestep and each column corresponding to one site)
*Bunit*: scaling factor with which the magnetic field must be multiplied to get it in nT (scalar)
$year, month, day$: UT date of the event (scalars)
$t$: UT in decimal hours (vector of length $N$)
$interval$: time step in seconds between successive observations (scalar)
$lat, long$: geographic latitudes and longitudes of the surface grid points (vectors of length $M$)
*names*: names of the grid point "stations" (string array with $M$ rows)

Some variables (*baseline, baselinestring*) are not needed here, but the binary file is intentionally in the format used at FMI in other studies. Quiet time baselines are subtracted from the data used in this study. Baselines are selected visually for each event. This is a satisfactory method, since concerning large variations, the exact selection criteria for a quiet time are not critical.

The calculated electric field is also saved as MatLab binary files named as exey_irf_YYYYMMDD.mat, and containing the following variables:

$EX, EY$: geographic north and east components of the electric field ($NxM$ matrices, each row corresponding to one timestep and each column corresponding to one site)
*Bunit*: scaling factor with which the electric field must be multiplied to get it in mV/km (scalar)
$year, month, day$: UT date of the event (scalars)
$t$: UT in decimal hours (vector of length $N$)
$T$: time step in seconds between successive observations (scalar)
$lat, long$: geographic latitudes and longitudes of the surface grid points (vectors of length $M$)
*mywindow*: window function multiplying the input magnetic field time series

(vector of length $N$)
*thick*: thicknesses of the earth layers [m]; note that the lowest layer has an infinite depth and is not included in this vector of length $P-1$
*sigma*: conductivities of the earth layers in 1/ohmm (vector of length $P$)
*myy*: permeabilities of the earth layers in SI units (vector of length $P$); reasonable values are equal to the vacuum permeability
*epsilon*: permittivities of the earth layers in SI units (vector of length $P$); due to the insignificance of the displacement current in the earth, exact values are not needed

Measured GIC are given in a single ASCII file with each line containing the following data values: year month day hour minute second GIC. Time is given in UT and GIC in amperes. The same data are also available as a single MatLab binary file containing one data matrix with the same format as given above.

# 5 Discussion

This study has shown that modelling of GIC in the southern part of the Swedish power system is feasible even with partly imperfect input data. There were no geomagnetic recordings available at the area of the power grid, but we could interpolate and extrapolate the field for the study region with data from other observatories. The qualitative fit between the modelled and measured GIC is satisfactory.

To make the model quantitatively better, geomagnetic recordings at the area are necessary. This is in progress with a magnetometer being installed in Växjö. It will be located close to the middle of the power system. Then it is obviously possible to use that single site to calculate GIC with a good accuracy with the assumption of a spatially uniform electric field. This would resemble the Finnish GIC Now! system for a natural gas pipeline network.

## Acknowledgements

The FMI contribution to this SDA is to a great extent based on experiences obtained in Finland. Fingrid Oyj has contributed to studies on geomagnetically induced currents in the Finnish high voltage power system for nearly 30 years. Especially, we would like to thank Mr. Jarmo Elovaara and Mr. Matti Lahtinen for their continuous interest in our work. Part of the network mod-

elling was performed during a short-term scientific mission by Risto Pirjola to Lund within the COST 724 action.

# 6 References

Korja, T., M. Engels, A.A. Zhamaletdinov, A.A. Kovtun, N.A. Palshin, M.Yu. Smirnov, A.D. Tokarev, V.E. Asming, L.L. Vanyan, I.L. Vardaniants, and the BEAR Working Group, Crustal conductivity in Fennoscandia - a compilation of a database on crustal conductance in the Fennoscandian Shield, *Earth Planets Space*, **54**, 535–558, 2002.

Lehtinen, M. and R. Pirjola, Currents produced in earthed conductor networks by geomagnetically-induced electric fields. *Ann. Geophys.*, **3**, 479–484, 1985.

Pirjola, R., Effects of space weather on high-latitude ground systems. *Adv. Space Res.*, **36**, doi:10.1016/j.asr.2003.04.074, 2231-2240, 2005.
Pulkkinen, A., Geomagnetic induction during highly disturbed space weather conditions: Studies of ground effects. *Finnish Meteorological Institute Contributions*, **42**, 164 p., 2003.

Pulkkinen, A., O. Amm, A. Viljanen and BEAR Working Group, Ionospheric equivalent current distributions determined with the method of elementary current systems. *J. Geophys. Res.*, **108**, doi: 10.1029/2001JA005085, 2003a.

Pulkkinen, A., A. Thomson, E. Clarke, and A. McKay, April 2000 geomagnetic storm: ionospheric drivers of large geomagnetically induced currents. *Ann. Geophys.*, **21**, 709–717, 2003b.

Viljanen, A. and R. Pirjola, Statistics on geomagnetically-induced currents in the Finnish 400 kV power system based on recordings of geomagnetic variations. *J. Geomag. Geoelectr.*, **41**, 411–420, 1989.

Viljanen, A., H. Nevanlinna, K. Pajunpää and A. Pulkkinen, Time derivative of the horizontal geomagnetic field as an activity indicator. *Ann. Geophys.*, **19**, 1107–1118, 2001.

Viljanen, A., A. Pulkkinen, O. Amm, R. Pirjola, T. Korja and BEAR Working Group, Fast computation of the geoelectric field using the method of elementary current systems and planar Earth models. *Ann. Geophys.*, **22**, 101–113, 2004.